Journal of Power Sources 229 (2013) 117–122

Contents lists available at SciVerse ScienceDirect

Journal of Power Sources

journal homepage: www.elsevier.com/locate/jpowsour

A structural, spectroscopic and electrochemical study of a lithium ion conducting $Li_{10}GeP_2S_{12}$ solid electrolyte

Jusef Hassoun [a,*], Roberta Verrelli [a], Priscilla Reale [a], Stefania Panero [a], Gino Mariotto [b], Steven Greenbaum [c,*], Bruno Scrosati [a]

[a] Sapienza University of Rome, Chemistry Department, 00148 Rome, Italy
[b] University of Verona, Computer Science Department, 37134 Verona, Italy
[c] Hunter College of the City University of New York, Department of Physics & Astronomy, New York, NY 10065, USA

HIGHLIGHTS

- Detailed spectroscopic and electrochemical evaluation $Li_{10}GeP_2S_{12}$ is presented.
- A Li^+ transference number of unity has been unambiguously confirmed.
- Tests were carried out with metallic Li and $LiFePO_4$ or $LiNi_{0.5}Mn_{1.5}O_4$ electrodes.

ARTICLE INFO

Article history:
Received 12 September 2012
Received in revised form
15 November 2012
Accepted 29 November 2012
Available online 10 December 2012

Keywords:
$Li_{10}GeP_2S_{12}$
Solid electrolyte
XRD
Raman
Lithium battery

ABSTRACT

In this paper we report an X-ray diffraction (XRD), Raman spectroscopy and electrochemical study of the $Li_{10}GeP_2S_{12}$ lithium ion conducting solid electrolyte. The XRD results confirm the structure of the electrolyte, the Raman spectroscopy evidences the composite nature of the solid solution showing some spectral features typical of the starting Li_2S, GeS_2, and P_2S_5 materials, whereas a band peaked at about 495 cm^{-1} is identified as the specific fingerprint of the $Li_{10}GeP_2S_{12}$ compound. The electrochemical studies, involving impedance spectroscopy, scan voltammetry and chrono-amperometry, demonstrate an ionic conductivity of the order of 10^{-3} S cm^{-1} over a wide temperature range with activation energy of approximately 0.1 eV, lithium transference of 0.99 and a stability window extending from 0 V to 6 V vs. Li. Further tests yield preliminary results obtained by Potentiodynamic Cycling with Galvanostatic Acceleration (PGCA) evaluation, which were carried out on a lithium metal anode as well as on lithium iron phosphate $LiFePO_4$ and lithium nickel manganese oxide $LiNi_{0.5}Mn_{1.5}O_4$ cathodes in cells using $Li_{10}GeP_2S_{12}$ as electrolyte. The material properties described above in conjunction with these tests identify $Li_{10}GeP_2S_{12}$ as a very promising electrolyte for the development of advanced solid-state batteries.

1. Introduction

Solid ionic lithium conductors are interesting materials since they may allow the development of solid-state, reliable lithium batteries. Interesting examples are glassy compounds of the thiolisicon family, such as Li_2S–P_2S_5, Li_2S–SiS_2 and Li_2S–GeS_2–P_2S_5 [1–3]. Their conductivity, however, although higher than other solids, is still too low for practical use. Other solid electrolytes of glassy or ceramic form have been successfully incorporated into thin film batteries. For example, lithium phosphonitride glass (LIPON) can be prepared by a variety of techniques and its mechanical and electrical properties have made it the dominant solid electrolyte in planar thin film configurations [4,5]. More recent work has demonstrated that LIPON can be also deposited in a conformal 3-D microbattery (3DMB) format. [6] However, the room temperature conductivity of the LIPON electrolyte has been reported to be very low, i.e. of the order of 2×10^{-6} S cm^{-1}.

Recently, high Li^+ conductivity solid electrolytes with a NASICON-type crystalline phase, consisting of a Li_2O–Al_2O_3–SiO_2–P_2O_5–TiO_2–GeO_2 composite (LISICON) [7], have been reported with room temperature Li^+ conductivities of 10^{-3}–10^{-4} S cm^{-1}. These solid electrolytes demonstrated acceptable air stability, but low chemical stability against metallic lithium. Some success with stabilizating the Li-NASICON electrolyte interface by sputtering a passive LiPON film on the surface of the electrolyte was reported,

* Corresponding authors. Tel.: +1 212 772 4973; fax: +1 212 772 5390.
E-mail addresses: jusef.hassoun@uniroma1.it (J. Hassoun), steve.greenbaum@hunter.cuny.edu (S. Greenbaum).

0378-7753/$ – see front matter © 2012 Elsevier B.V. All rights reserved.
http://dx.doi.org/10.1016/j.jpowsour.2012.11.130

leading to an electrolyte with a lower room temperature conductivity, i.e. on the order of 1×10^{-4}, but with a higher chemical and electrochemical stability versus metallic lithium [4].

A renewed interest in solid electrolytes has arisen by the recent discovery of the $Li_{10}GeP_2S_{12}$ compound, reported as a solid having a mono-dimensional conduction pathway exhibiting a very high ionic conductivity, i.e. of about 9×10^{-3} S cm^{-1} at room temperature. [8] The short-range structural and electrochemical characteristics $Li_{10}GeP_2S_{12}$, however, are not yet totally clear. Important transport parameters pertaining to lithium battery performance such as lithium diffusion coefficient and lithium transference number are still missing; hence, it has appeared to us of interest to provide these details by carrying out a thorough investigation of this compound using a combination of complementary analyses, including X-ray diffraction (XRD), Raman spectroscopy, electrochemical impedance spectroscopy and sweep voltammetry. In this work we studied important electrochemical properties of the $Li_{10}GeP_2S_{12}$ electrolyte, including the lithium transference number, the electronic conductivity, and the lithium metal–electrolyte interface. These parameters, to our knowledge here determined for the first time, are of key importance in the evaluation of the feasibility of the material as an electrolyte for solid-state lithium batteries, such as those using lithium iron phosphate, LFP or lithium nickel manganese spinel, LNMO as cathodes, as clearly demonstrated in this work.

2. Experimental

2.1. Synthesis

Following Ref. 8, Li_2S (Aldrich, 99%), P_2S_5 (Sigma–Aldrich, 99%) and GeS_2 (City Chemical LLC, 99.99%) were used as starting materials.

The precursors used for the electrolyte synthesis were highly pure. No evaporation or contamination occurred during the synthesis, due to the high purity of the argon atmosphere (99.999%).

Operating in an Ar-filled glove box, these reagents were mixed together in the molar ratio $Li_2S/P_2S_5/GeS_2 = 5/1/1$ and were subjected to a mechano-chemical treatment for 6 h using a high energy spex milling apparatus (Retsch Mixer Mill MM400). The powder obtained was then pressed into pellets and sealed in a quartz tube. The pressed density of the pellet was of the order of 2 g cm^{-3}.

The sample was then annealed at 550 °C for 8 h under Ar flowing in a furnace (Argon purity of the order of 99.999%). The heating rate was 5 °C min^{-1} while the cooling was not rate-controlled.

2.2. XRD and Raman measurements

XRD analyses were performed using a Rigaku D-max Ultima + X-ray diffractometer with Cu-Kα radiation source, holding the sample in a quartz capillary of 0.4 mm diameter, sealed under Ar atmosphere.

Unpolarized micro-Raman spectra from the $Li_{10}GeP_2S_{12}$ powders, sealed into an evacuated quartz capillary, were carried out at room temperature in backscattering geometry using a microprobe set-up (Horiba-Jobin Yvon, model Labram HR), equipped with holographic gratings having 1800 lines/mm. The scattered radiation was detected at the spectrograph output by a charge coupled device (CCD) detector, with 1024 × 256 pixels, cooled by liquid nitrogen. The spectra were excited by the 632.8 nm line of an He–Ne laser focused on the surface of the sample through the capillary with a spot of about 1 μm obtained by using the lens of an objective 80X (NA = 0.75). The power at the capillary surface was less than 3 mW. Repeated micro-Raman measurements were carried out under the same experimental conditions from different points of the capillary filled with the nanocrystalline powders and the spectra showed a good reproducibility, thus suggesting a high degree of homogeneity of the treated powders. The experimental spectra were superimposed on a quite strong luminescence signal, in form of a continuously increasing and structureless background, underlying the overall Raman spectrum, but clearly distinguishable from it.

2.3. Electrochemical tests

A VersaSTAT MC multi-channel potentiostat-galvanostat (Princeton Applied Research) was used for the tests. The $Li_{10}GeP_2S_{12}$ powder was pressed into pellets with a diameter of 12 mm and a thickness ranging from 0.4 to 0.6 mm for the different cells that we made. However, each cell had its own electrolyte thickness determined with an error of 0.005–0.01 mm, i.e. of about 2%. The ionic conductivity was determined in cooling scans from 120 °C to room temperature by Electrochemical Impedance Spectroscopy, EIS, run on a symmetric Al/$Li_{10}GeP_2S_{12}$ pellet sample/Al cell, applying 30 mV in the frequency range 100 kHz–50 Hz. Linearization of the experimental data was performed in order to determine the conduction activation energy. The linearization parameters are reported in Table 1.

The electrochemical stability window, ESW, was measured by Linear Sweep Voltammetry run on Li/$Li_{10}GeP_2S_{12}$ pellet sample/Super P (anodic scan) and Li/$Li_{10}GeP_2S_{12}$ pellet sample/Cu (cathodic scan) cells in a voltage range from −0.5 V to 6 V vs. Li/Li$^+$ and with a 0.1 mV s^{-1} scan rate.

The lithium transference number was determined by a chronoamperometry test on a Li/$Li_{10}GeP_2S_{12}$ pellet sample/Li cell with an applied 0.5 V voltage. The test was completed by EIS measurements taken before and after the polarization scans in accordance with the method proposed by Bruce and Vincent. [9] EIS measurements for the lithium transference number determination were performed applying a potential of 30 mV in the frequency range 1 MHz–50 Hz. The lithium diffusion coefficient was derived by impedance spectra of a symmetric Li/$Li_{10}GeP_2S_{12}$ pellet sample/Li cell and the Li stripping/deposition kinetics by 0.1 mA galvanostatic cycles on the same cell using a Maccor Series 4000 Battery Test System (Maccor, Inc.).

Potentiodynamic Cycling with Galvanostatic Acceleration (PCGA), a quasi-thermodynamic analysis [10], was carried out with $LiFePO_4$ and $LiNi_{0.5}Mn_{1.5}O_4$ electrode powders in lithium cells using the $Li_{10}GeP_2S_{12}$ solid electrolyte at room temperature. Electrode, electrolyte and Super P carbon powders were mixed in the ratio of 6:2:2, pressed on top of a $Li_{10}GeP_2S_{12}$ pellet previously formed, and conditioned under argon at 150 °C for 3 h in order to enhance the contact at the electrode–electrolyte interface. The electrode–electrolyte pellet assembly was then cooled back to ambient temperature, and coupled with lithium metal in a Swagelok cell to perform the PCGA test, setting stepwise potential scans of 5 mV with a minimum current limit of 1 μA, within 2–4 V and 3.3–5.5 V vs. Li voltage ranges for the $LiFePO_4$ and the $LiNi_{0.5}Mn_{1.5}O_4$ electrodes, respectively, using a Bistat Biologic-Science Instruments.

Table 1
Parameters determined from the linear fit of the experimental Arrhenius conductivity plot. P and C are, respectively, the slope and the intercepts of the linear plot of equation $y = Px + C$. R is the confidence coefficient of the linearization, SD is the standard deviation and N is the number of points considered.

P	C	R	SD	N
−0.75018	−1.25583	−0.89135	1.14773	8

3. Results and discussion

Fig. 1 displays the XRD pattern of our $Li_{10}GeP_2S_{12}$ electrolyte sample, essentially confirming the well-defined structure of a one-dimensional Li-conducting lattice as already reported in the literature. [8] The Rietveld refinement of the XRD pattern indicated a contaminant amount lower than 3% in the electrolyte, a crystallite size of 723 ± 21 Å and the following cell parameters: $a = 8.708 \pm 0.001$ Å and $c = 12.615 \pm 0.006$ Å (lattice tetragonal, space group $P4_2/nmc$).

Work is in progress in our laboratory to upgrade the synthesis conditions, e.g., by optimizing time and temperature, in order to further reduce or even eliminate any trace of the contaminant.

Fig. 2 (top panel) shows a typical unpolarized micro-Raman spectrum carried out in the region between 200 cm^{-1} and 750 cm^{-1} from $Li_{10}GeP_2S_{12}$, sealed in an evacuated quartz capillary. Hereafter, we shall discuss its spectral features with regard to corresponding features observed in starting component materials and, in particular, the $Li_2S–P_2S_5$ solid solution. To this aim, the spectrum of this solid solution, carried out under the same experimental conditions, is also reported in Fig. 2 (bottom panel).

At first glance, the spectra of the two compounds display some common features, in form of partially overlapping peaks and bands with somewhat different relative intensities. However, a finer analysis provides evidence of subtle differences which are intimately related to the powder composition and phases. For instance, the most intriguing spectral feature is the peak centered at about 420 cm^{-1}, which turns out to be much broader (about a factor of two) in $Li_{10}GeP_2S_{12}$ powder than in the $Li_2S–P_2S_5$. Based on literature data [11], this difference can be interpreted as the convolution of the scattering components due to the stretching vibrations of $(P_2S_7)^{4-}$, $(\equiv Ge–S^-)$ and $(PS_4)^{3-}$ units, occurring respectively at 410, 415 and 420 cm^{-1}. The comparison with the $Li_2S–P_2S_5$, i.e. of a phase already well-investigated [12], suggests that the main contribution to the peak at 420 cm^{-1} comes from the stretching mode of $(PS_4)^{3-}$ units. On the other hand, in $Li_2S–P_2S_5$ powder, the band centered at about 390 cm^{-1}, which appears as a shoulder of the main peak at 420 cm^{-1}, is attributed to P–P stretching of the $P_2S_6^{4-}$ units, while the broad and very weak band at about 475 cm^{-1} is likewise due to S–S stretching of Li_2S starting compound [12]. No evidence of these two bands can be observed upon inspection of the spectrum of the $Li_{10}GeP_2S_{12}$ powder, in which, besides the main peak centered at 420 cm^{-1}, three additional peaks are observed at about 345 cm^{-1}, 367 cm^{-1} and 384 cm^{-1}, respectively. Among them, the peak at ~367 cm^{-1} is assigned to the $Li^+–S^-$ stretching mode. As reported in the literature [13,13a,13b] a nearby peak at about 372 cm^{-1} can be found in the spectrum of pure Li_2S, for which an additional very broad and weak band was also observed at about 460 cm^{-1} [13,13b]. In turn, the peak at about 345 cm^{-1} occurring in the Raman spectrum of $Li_{10}GeP_2S_{12}$ should be associated with the symmetric stretching mode of the tetrahedral $(GeS_{0.5})_4$ group, according to Lucovsky et al. [14]. Finally, the peak at about 384 cm^{-1} is attributed to a $(GeS_{0.5}S_3)^{3-}$ unit with non-bridging sulfur [13]. In brief, on the basis of the present measurements, it is not possible to ascertain if these three peaks are due inherently to the $Li_{10}GeP_2S_{12}$ compound or to the GeS_2 and Li_2S starting materials, surviving as separated phases in the $Li_{10}GeP_2S_{12}$ solid solution. As mentioned, direct XRD evidence of the starting materials is inconclusive. In spite of this, the broad band peaked at about 495 cm^{-1}, not observed in the Raman spectra of any of the starting materials, is specific to $Li_{10}GeP_2S_{12}$ and is regarded as an unambiguous fingerprint of this compound.

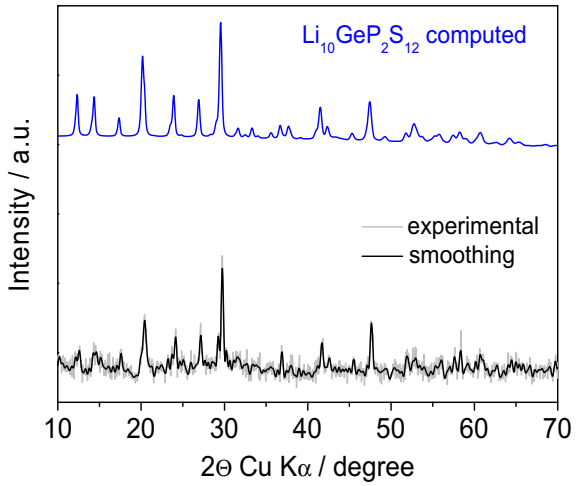

Fig. 1. X ray diffraction patterns (XRD) of the $Li_{10}GeP_2S_{12}$ solid electrolyte.

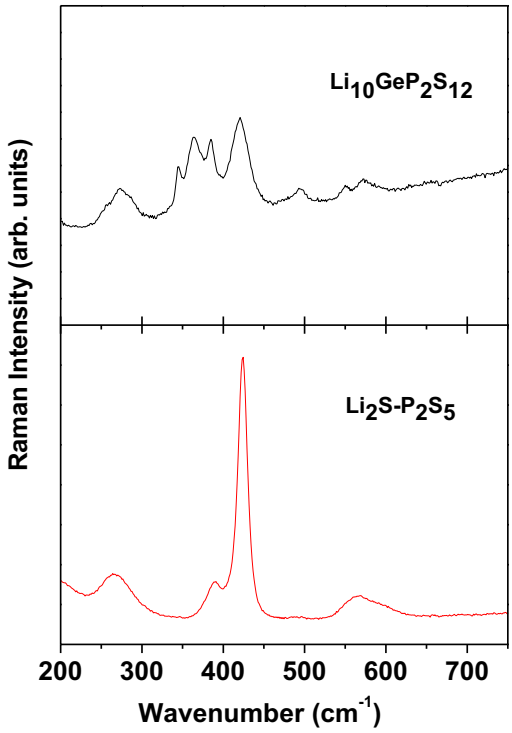

Fig. 2. Unpolarized micro-Raman spectra carried out from the $Li_{10}GeP_2S_{12}$ solid electrolyte (upper panel) and from the $Li_2S–P_2S_5$ solid solution (lower panel). Measurement details: excitation at 632.8 nm, powder sealed into the capillary tube, backscattering geometry.

Fig. 3A shows the Arrhenius conductivity plot of the $Li_{10}GeP_2S_{12}$ electrolyte revealing an ionic conductivity of the order of 10^{-3} S cm^{-1} over the entire temperature range from 20 °C to 110 °C, similar (though somewhat lower) to that previously reported. This is a very high value approaching that of the organic electrolyte solutions commonly used in lithium ion batteries, confirming the practical relevance of the $Li_{10}GeP_2S_{12}$ electrolyte.

The Al/Electrolyte/Al blocking electrode cell used for this analysis shows resistance values of the order of hundreds of ohms, due to the contribution of only the electrolyte. Representative Nyquist plots of the cell analyzed are displayed Fig. 3B.

From the Arrhenius plot of Fig. 3A the activation energy for the ionic transport is calculated as be 0.065 eV, i.e. a very low value that

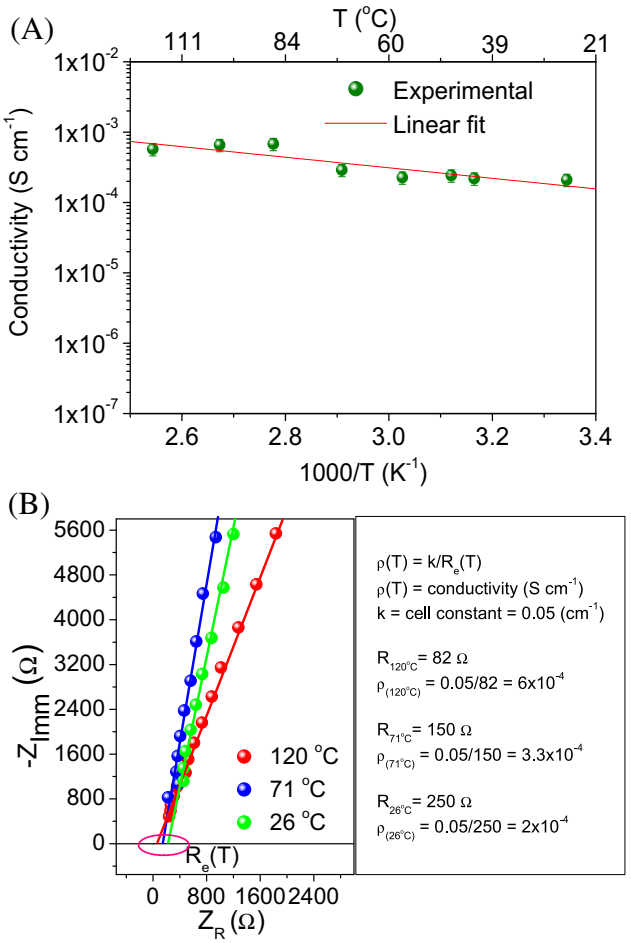

Fig. 3. (A) Arrhenius conductivity plots of the $Li_{10}GeP_2S_{12}$ electrolyte studied in this work. Data obtained by impedance spectroscopy. (B) Several representative Nyquist plots and corresponding conductivity determination.

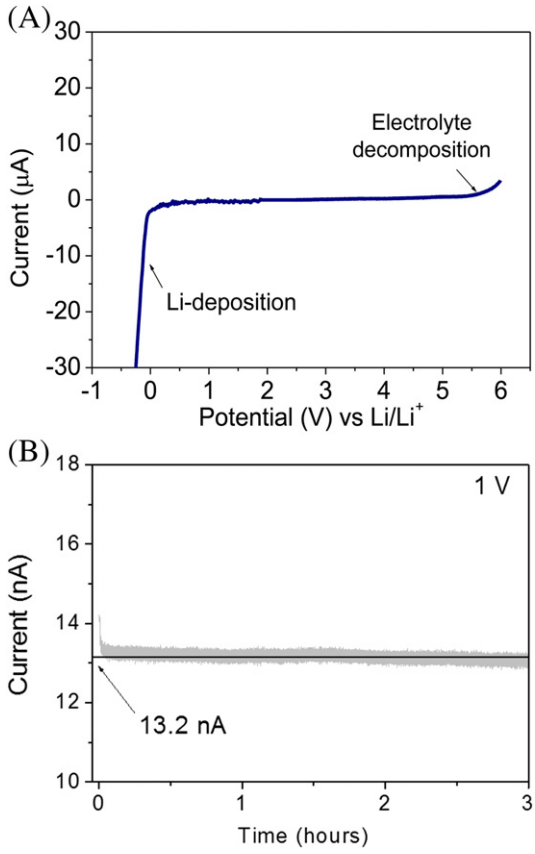

Fig. 4. (A) Current-potential curve of a Super P carbon electrode (anodic range) and of a copper electrode (cathodic range) in a lithium $Li_{10}GeP_2S_{12}$ electrolyte cell. (B) Current profile of a cell polarized at 1 V under blocking conditions. $Li_{10}GeP_2S_{12}$ electrolyte. Room temperature.

is consistent with the fast lithium ion transport in the solid $Li_{10}GeP_2S_{12}$ material.

Fig. 4A displays the current–potential curve of a Super P carbon electrode in a lithium cell using the $Li_{10}GeP_2S_{12}$ electrolyte. Since the electrode is of the blocking type, the onset of the current is necessarily associated with electrolyte decomposition. The results demonstrate that the stability in the anodic range extends to about 5.9 V vs Li, indicating that the $Li_{10}GeP_2S_{12}$ electrolyte may be used in lithium cells employing high voltage cathodes, such as $LiNi_{0.5}Mn_{1.5}O_4$ [15]. The cathodic limit of the electrolyte stability is equal to − 0.2 V vs. Li^+, likely corresponding to the process of lithium deposition on the copper electrode.

Fig. 4B shows the current–time profile of a cell using a Stainless Steel (SS) blocking-electrode following a 1 V polarization. The current, that under the given cell condition can be only of electronic origin, stabilizes at about 13 nA. Taking into account a cell constant of 0.05 cm^{-1}, one obtains an electronic conductivity of 6.5×10^{-10} S cm^{-1}, i.e. a value about 6 orders of magnitude lower than the ionic one, and comparable with that reported in literature for similar solid ionic materials [16].

Fig. 5 reports the chrono–amperometric profile of a symmetric $Li/Li_{10}GeP_2S_{12}/Li$ cell used for the lithium transference number determination in the solid electrolyte. Under a dc polarization of 0.5 V, the current exhibits only a small decay with time. The initial and final, steady value of the current are I_0 = 190 μA and I_{ss} = 175 μA, respectively. We registered a very low initial current of 0.8 μA followed by a very fast activation process to reach the maximum current of 190 μA. The Li/Electrolyte/Li cell analyzed shows an impedance response characterized by the contribution of the electrolyte resistance (intercept of the semicircle at the higher frequencies) and the lithium-interphase resistance (diameter of the semicircle). Thick electrolyte was used in order to avoid a Li/Li short circuit.

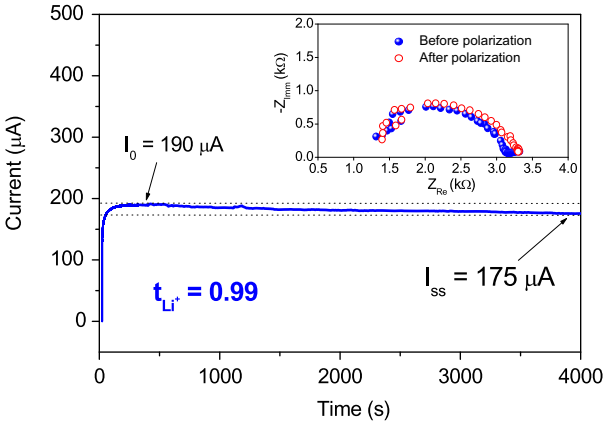

Fig. 5. Chrono-amperometric profile of a $Li/Li_{10}GeP_2S_{12}/Li$ symmetrical cell polarized at 0.5 V. I_o = initial current; I_{ss} = final steady current. Inset: impedance spectra performed before and after cell polarization.

Taking into account the effects of the polarization over the electrode/electrolyte interphase, t_{Li}^{+} is calculated by using the exact Bruce–Vincent–Evans equation [9] as:

$$t_{Li}^{+} = \frac{I_{SS}(\Delta V - I_0 R_0)}{I_0(\Delta V - I_{SS}R_{SS})}$$

where I_0 and I_{SS} are, respectively, the initial and stationary state current, ΔV is the applied voltage and R_0 and R_{SS} are the interphase resistance values before and after polarization. The impedance responses of the cell prior and after polarization differ only slightly from each other: $R_0 = 2545\ \Omega$ and $R_{SS} = 2580\ \Omega$. Using this method, we evaluate a lithium transport number of 0.99. The equivalent circuit used to describe the symmetrical Li/$Li_{10}GeP_2S_{12}$/Li cell examined in Fig. 5 was of the type Re($R_{int}Q_{int}$), where R_e represented the electrolyte resistance and the circuit elements ($R_{int}Q_{int}$) accounted for the various phenomena associated with the electrolyte/electrode interface.

We recall here that lithium ion batteries operate with an intercalation chemistry where lithium is the only carrier being shuttled from the cathode to the anode [17]. Some of the commonly used organic electrolytes, especially those having low-size anions, although characterized by comparable values of ionic conductivity, suffer from a lithium transference number that is much lower than unity, i.e., generally of the order of 0.3. This low value results in a serious concentration polarization upon cell operation, finally affecting the rate capability of the battery. The use of an electrolyte with a t_{Li}^{+} approaching unity would then be greatly beneficial for the progress of the lithium battery technology, not only in terms of rate capability but also, and equally important, in terms of safety since the solid electrolyte is certainly much less reactive than the flammable organic carbonates. It is not suggested here that a solid electrolyte as the present compound would be applicable to large format (i.e. EV) batteries because of electrical contact problems inherent to ceramic materials, but safety issues are still paramount, especially in high energy density configurations as the 3DMB.

Fig. 6 shows the impedance response of a symmetric Li/$Li_{10}GeP_2S_{12}$/Li cell extended to the very low frequency range, i.e. to 0.1 Hz. Generally, the lithium metal electrode surface is slightly passivated and lithium ions can diffuse from the electrolyte to the surface film without appreciable limitation, and the resulting impedance is of the Warburg type. However, if the Li surface passivation layer is inhomogeneous or has a porous structure in which some of the pores are filled by electrolyte, as expected in our conditions, the diffusion process is limited, and this results in a deformation of the Warburg impedance to a depressed loop-type profile [18]. The non-linear least square (NLLS) analysis of the spectra allows one to calculate the diffusion impedance (R_W) and, consequently the lithium diffusion coefficient [19] according to Warburg equation:

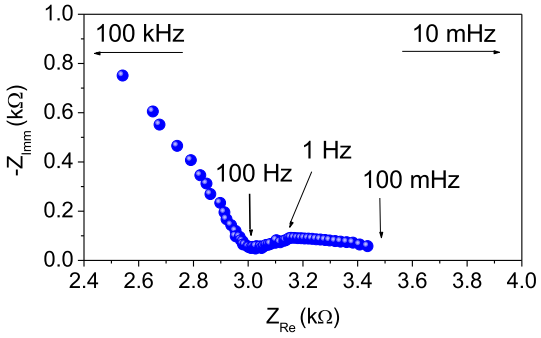

Fig. 6. Nyquist impedance plot of a Li/$Li_{10}GeP_2S_{12}$ electrolyte/Li symmetric cell. Frequency range: 100 kHz–0.1 Hz; ac signal amplitude: 100 mV. Measurements performed at room temperature.

$$R_W = \frac{RT}{n^2F^2C_l\sqrt{2\theta D}} \quad (1)$$

where R is the gas constant (8.314 J K^{-1} mol^{-1}), F is the Faraday constant (96,485 C mol^{-1}), T is the temperature (298 K), n is the charge number of the mobile specie (1 for Li^+), C_l is the linear concentration of mobile specie (0.0028 mol cm^{-1} for Li^+ in the prepared $Li_{10}GeP_2S_{12}$ pellet), Θ is the final frequency of the measurement (0.1 Hz in Fig. 6), R_w is Warburg resistance (calculated by NLLS from Fig. 6 as 83 Ω) and D is the lithium-diffusion coefficient (in cm^2 s^{-1}) in the $Li_{10}GeP_2S_{12}$ solid electrolyte. The experimental impedance data of the Li/$Li_{10}GeP_2S_{12}$/Li cell examined in Fig. 6 were determined using an equivalent circuit composed of the electrolyte bulk resistance R_e, and ($R_{int}Q_{int}$) elements accounting for all the phenomena associated with the electrolyte/electrode interface and a Warburg-type element related to the diffusion process. The frequency dependence of the impedance deviates from a typical Warburg-type behavior: this deviation, as discussed in an already cited reference, [18] arises from the inhomogeneities and porosity of the Li electrode surface.

By the Equation (1), we obtain $D = 6.7 \times 10^{-12}$ cm^2 s^{-1}, i.e. a value typically expected in solid ionic conductors [20]. Using this D value in the Nernst–Einstein equation [21]:

$$k = zuFC_0 = \frac{z^2DF^2C_0}{RT} \quad (2)$$

where k is the ionic conductivity (S cm^{-1}), z is the charge of the mobile specie (+1), u is the mobility of the ion (S cm^2 C^{-1}), F is the Faraday constant (96,485 C mol^{-1}), T is the temperature (298 K), R is the gas constant, C_0 is the electrolyte concentration (mol cm^{-3}) multiplied by 1000, one may calculate the room temperature conductivity of the $Li_{10}GeP_2S_{12}$ solid electrolyte as equal to 0.8×10^{-4} S cm^{-1}, i.e. a value slightly lower than that determined by the Arrhenius plot of Fig. 3. This difference can be explained by considering the Haven correlation factor (f) of the Nernst–Einstein equation given as: $f = DF^2C_0/\sigma RT$, where DF^2C_0/RT represents the calculated conductivity (k, see Equation (2)) and σ is the experimental value of conductivity, see Fig. 3, i.e., $f = k/\sigma = 0.8 \times 10^{-4}/2 \times 10^{-4} = 0.4$.

It is important to remark that that the correlation factor f can vary between 0 and 1 depending on the type of diffusion mechanism of the mobile ion [22,23]. For instance, in crystalline materials an f value approaching zero is associated with a vacancy-regulated diffusion mechanism, while $f \approx 1$ describes migration by sequences of uncorrelated jumps via interstitials [1,24–26].

Accordingly, the f factor for the $Li_{10}GeP_2S_{12}$ electrolyte here under study suggests a Li diffusion primarily through a vacancy mechanism with strongly correlated lithium ion motion, similar to that determined for single ion diffusion in solid glass electrolytes [26,27].

A galvanostatic deposition-stripping test carried out in a symmetric Li/$Li_{10}GeP_2S_{12}$/Li cell demonstrates low polarization values and a good cycling stability of the lithium electrode in the solid electrolyte cell, see Fig. 7A, confirming the applicability of $Li_{10}GeP_2S_{12}$ in advanced, solid state lithium batteries. This is further strengthened by comparing the trend of lithium deposition/stripping on a copper substrate with those of the potentiodynamic cycling with galvanostatic acceleration (PCGA) test of a lithium iron phosphate $LiFePO_4$ and a lithium nickel manganese oxide $LiNi_{0.5}Mn_{1.5}O_4$ (LMNO) electrodes in lithium cells using the $Li_{10}GeP_2S_{12}$ electrolyte, as can be seen in Fig. 7B. The results show

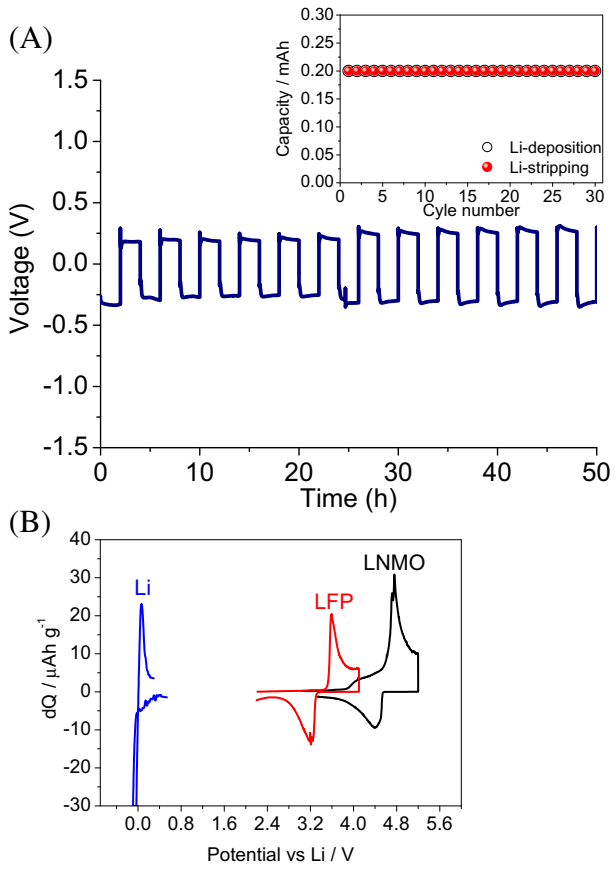

Fig. 7. (A) Overvoltage vs. time for galvanostatic lithium deposition-stripping cycles in a Li/$Li_{10}GeP_2S_{12}$/Li symmetric cell. Current: 0.1 mA; room temperature. Inset: capacity vs. cycle number. (B) Voltammetric profile of the lithium deposition-stripping on cupper substrate and differential capacity versus potential profile of the potentiodynamic cycling with galvanostatic acceleration (PCGA) test of the $LiFePO_4$ (LFP) and $LiNi_{0.5}Mn_{1.5}O_4$ (LNMO) electrodes in lithium cells using the $Li_{10}GeP_2S_{12}$ electrolyte. Measurements performed at room temperature.

that the Li electrode, as well as the LFP and LNMO electrodes cycle well, with low polarization and fast kinetics and with the expected voltage signatures, centered at about 3.5 V and 4.7 V vs. Li, [28,29] respectively, suggesting that the electrodes may be combined to form efficient Li/$Li_{10}GeP_2S_{12}$/LFP and Li/$Li_{10}GeP_2S_{12}$/$LiNi_{0.5}Mn_{1.5}O_4$ solid state batteries.

4. Conclusion

In this work we have carried out a detailed electrochemical characterization of the recently discovered $Li_{10}GeP_2S_{12}$ solid electrolyte by reporting, to our knowledge for the first time, important parameters such as activation energy for lithium ion transport, lithium ion transference number and lithium ion diffusion coefficient. Furthermore, we demonstrated the compatibility of the $Li_{10}GeP_2S_{12}$ solid electrolyte with the $LiFePO_4$ olivine and the $LiNi_{0.5}Mn_{1.5}O_4$ high voltage spinel cathode. We believe that such characterization at this level of detail may greatly contribute to the consideration of this compound as an effective, new electrolyte for advanced, solid-state batteries.

Acknowledgments

This work was carried out within the SEED Project "REALIST" sponsored by Italian Institute of Technology (IIT). One of us (SG) acknowledges the U.S. Department of Energy, Division of Basic Energy Sciences for salary support during his sabbatical leave from Hunter College.

References

[1] F. Mizuno, A. Hayashi, K. Tadanaga, M. Tatsumisago, Adv. Mater. 17 (2005) 918.
[2] S. Kondo, K. Takada, Y. Yamamura, Solid State Ionics 53 (1992) 1183.
[3] R. Kanno, M. Murayama, J. Electrochem. Soc. 148 (2001) A742.
[4] W.C. West, J.F. Whitacre, J.R. Lim, J. Power Sources 126 (2004) 134–138.
[5] N.J. Dudney, J. Power Sources 89 (2000) 176.
[6] F. Xu, N.J. Dudney, G.M. Veith, Y. Kim, C. Erdonmez, W. Lai, Y.M. Chiang, J. Mater. Res. 25 (2010) 1507.
[7] J. Fu, US Patent No. 5,702,995 (1997).
[8] N. Kamaya, K. Homma, Y. Yamakawa, M. Hirayama, R. Kanno, M. Yonemura, T. Kamiyama, Y. Kato, S. Hama, K. Kawamoto, A. Mitsui, Nat. Mater. 10 (2011) 682.
[9] J. Evans, C.A. Vincent, P.G. Bruce, Polymer 28 (1987) 2324.
[10] A.H. Thompson, J. Electrochem. Soc. 126 (1979) 608.
[11] K. Minami, A. Hayashi, M. Tatsumisago, J. Non-cryst. Solids 356 (2010) 2666.
[12] F. Mizuno, O. Takamasa, A. Hayashi, K. Tadanaga, M. Tatsumisago, Solid State Ionics 177 (2006) 2753.
[13] I. Seo, S.W. Martin, Inorg. Chem. 50 (2011) 2150;
(a) B. Bertheville, H. Bill, H. Hagemann, J. Phys. Condens. Matter 10 (1998) 2155;
(b) A. Grzechnik, A. Vegas, K. Syassen, I. Loa, M. Hanfand, M. Jansen, J. Solid State Chem. 154 (2000) 603.
[14] G. Lucovsky, J.P. deNeufville, F.L. Galeener, Phys. Rev. 9 (1970) 1591.
[15] J. Hassoun, S. Panero, P. Reale, B. Scrosati, Adv. Mater. 21 (2009) 4807.
[16] M. Murayama, N. Sonoyama, A. Yamada, R. Kanno, Solid State Ionics 170 (2004) 173.
[17] B. Scrosati, J. Garche, J. Power Sources 195 (2010) 2419.
[18] C. Fringant, A. Tranchant, R. Messina, Electrochim. Acta 40 (1995) 513.
[19] B.A. Boukamp, Solid State Ionics 18 (1986) 136.
[20] A.M. Welsch, H. Behrens, I. Horn, S. Ross, P. Heitjans, J. Phys. Chem. A 116 (2012) 309.
[21] J.L. Souquet, Solid State Ionics 40–41 (1990) 595.
[22] J.E. Kelly, J.F. Cordaro, M. Tomozawa, J. Non-cryst. Solids 41 (1980) 47.
[23] H. Mehrer, Diffusion in Solids Fundamentals, Methods, Materials, Diffusion-controlled Processes, vol. 155, Springer Series in Solid-State Sci, 2007, p.185.
[24] K. Compaan, Y. Haven, Trans. Faraday Soc. 52 (1956) 786.
[25] W. Beier, G.H. Frischat, J. Non-cryst. Solids 73 (1985) 113.
[26] T.B. Schroder, J.C. Dyre, Phys. Rev. Lett. 84 (2000) 310.
[27] B. Roling, Phys. Rev. B 61 (2000) 5993.
[28] P. Reale, S. Panero, B. Scrosati, J. Electrochem. Soc. 152 (2005) 1949.
[29] S.-W. Oh, S.-T. Myung, S.-M. Oh, K.-H. Oh, K. Amine, B. Scrosati, Y.-K. Sun, Adv. Mater. 22 (2010) 4842.